

Short Communication

The Characterisation of MWCNT-rGO-TiO₂ Nanocomposite as Potential Electrode Material for Hybrid Supercapacitor

Alif Daffa Setyoputra*, Heydar Ruffa, Heri Sutanto, Agus Subagio*

Physics Department, Science and Mathematics Faculty, Diponegoro University, Jl. Prof. Sudarto, SH, Tembalang, Semarang 50275, Indonesia

*E-mail: setyoputra02@gmail.com, agussubagio@lecturer.undip.ac.id

Received: 22 November 2021 / Accepted: 18 February 2022 / Published: 5 April 2022

Increasing energy demands are triggering the development of high performance, low-cost supercapacitor electrode material, particularly in countries that are shifting to renewable energy as their current energy supply cannot meet their significant energy demands. These countries require high-voltage, safe and long-lasting electrical energy storage devices. Multi-walled carbon nanotubes (MWCNTs), reduced graphene oxide (rGO) and Titanium Dioxide (TiO₂) were tested during an in-situ hydrothermal process. The structure test of X-ray diffraction (XRD) and scanning electron microscope (SEM) characterisation was used to determine the relation between the morphology of the electrode and its electrochemical value. The morphology of the composite electrode indicated that the nanocomposite electrode had better values than the single material electrode. Additionally, cyclic voltammetry (CV) and electrochemical impedance spectrum (EIS) tested in a two-electrode system indicated that the specific capacitance of MWCNT-rGO-TiO₂ 30% was 168 F g⁻¹ and showed the energy and power density to be 15 Wh kg⁻¹ and 337.5 W kg⁻¹, respectively. This result was higher with the other electrode due to the faradaic and non-faradaic processes in the electrode.

Keywords: MWCNT, rGO, TiO₂, hydrothermal method, morphology, electrochemical reaction, supercapacitor

1. INTRODUCTION

In the 21st century, the development of storage energy is the main concern for expanding the technology. Especially electronic devices such as cellular phones, laptops and electric vehicles that require an energy supply from an energy storage device. However, most batteries have low power density and a short life cycling time and take a long time to charge storage into the device. Thus, new technology is required that can provide a longer cycling time and greater energy and that can be charged in a short time. There is significant potential for energy storage devices and this field has generated great interest among researchers to develop more efficient energy storage devices. One such device is a supercapacitor

[1-3].

Supercapacitors have several important parts such as electrodes, a separator and electrolytes. Electrodes are an important aspect of supercapacitors that can ensure better performance at a low cost. The research on supercapacitor electrode materials includes carbon materials, metal oxides and conductive polymers and their composites. Multi-walled carbon nanotubes (MWCNTs) and reduced graphene oxide (rGO) have advantages regarding high specific capacitance, high conductivity and low cost. Carbon-based materials, including carbon nanotubes and activated carbon, have significant technological advantages for applications in energy storage [4-6]; most of the latest studies have used electrolytes such as 1 M H₂SO₄, 1 M Na₂SO₄, 6 M KOH and 1 M LiPF₆ [7-8].

There are three main types of supercapacitors with different energy storage mechanisms: electrochemical double-layer capacitors (EDLCs) are energy storage systems that use the charge accumulated at the interface between the electrolyte and electrodes, pseudo-capacitors (PDCs) store energy using a redox reaction and reversible faradaic on the surface of the electrode material and hybrid supercapacitors which is a combination of EDLCs and PDCs [9]. In recent years, supercapacitors have been developed by combining EDLCs with PDC using a hybrid system whereby both faradaic and redox reaction processes are used to store electrical charge [8,10]. Hybrid supercapacitors have high power and energy densities and long lifetimes [11] and use carbon material combined with metal oxide (MnO₂, TiO₂, SnO₂, Fe₃O₄, Fe₂O₃, RuO₂, CoS, CuS, Cu₂S, SnS₂ and NiCo₂S₄) [12]. Among the metal oxide materials, titanium dioxide (TiO₂) has many advantages due to its low toxicity, high stability, availability and beneficial physicochemical properties [13].

TiO₂ has been used in many applications, such as supercapacitors, fuel cells, batteries, photocatalysis, solar cells, sensors and water treatment. Its wide band-gap, photo-absorption properties and structural flexibility and the mobility of the charge carriers make TiO₂ a suitable solution to existing energy and environmental problems. One-dimensional TiO₂ nanostructures (tubes, wires, rods, etc.) have attracted great interest due to their high surface area to volume ratio, fast and long-distance electron transport properties, and high photoconductivity [13]. Several researchers have explored TiO₂ combined with composites such as graphene as the base material for supercapacitor electrodes. For example, Sun et.al. used a graphene sheet coated with TiO₂ nanoparticles with a specific capacitance yield of 75 F/g. Liu et.al. investigated a graphene oxide (GO)/TiO₂ hybrid electrode and reported a specific capacitance value of 100 F/g [4,14].

In this study, an MWCNT-rGO-TiO₂ electrode was synthesised using the doctor blade method. MWCNTs with reduced graphene oxide was combined with TiO₂ at several ratios, while the TiO₂ underwent an in-situ hydrothermal process and the graphene underwent an oxidation-reduction process to increase the life cycles so that MWCNTs, TiO₂ and rGO could increase the electrochemical value of the supercapacitor.

2. MATERIALS AND METHODS

2.1. Sample Preparation

The research method involved several stages: synthesis TiO₂, rGO, and purification of CNT material, the manufacture of a mixture of composite MWCNT-rGO-TiO₂, manufacture MWCNT-rGO-

TiO₂ thin film on the copper foil by doctor blade method, material characterisation, testing, and manufacturing of the prototype supercapacitor. Initially, 4 g TiO₂ was added with 70 ml NaOH 10 M and sonicated for 30 minutes. The mixture was transferred to a Teflon lined stainless steel autoclave and sealed in a hot air oven at 160 °C for 12 h for the hydrothermal process. Then, the solution was filtrated and distilled with DI water and placed in a furnace at a temperature of 600°C for 2 h to produce TiO₂ nanorods [13].

To make the rGO material, 2 g of graphite powder were added to 150 ml of sulfuric acid (H₂SO₄) and stirred until it formed a homogeneous graphite solution. While stirring in an ice bath to cool the solution, 7 g of potassium permanganate (KMnO₄) and then 200 ml of deionized water and 100 ml of hydrogen peroxide (H₂O₂) were added to produce an oxidation process. The stirring time was varied from 4 to 10 h to observe the effect of oxidation time on the pore structure of rGO. The activated rGO powder was transferred to the quartz tube and placed into a furnace under N₂ or argon condition at 600°C for 2 h [15]. Titanium dioxide (TiO₂) and graphene were purchased from MERCK Chemical Co. Ltd. All chemical reagents were in analytical grade and MWCNTs (inner diameter: 5–15 nm, outer diameter: >50 nm, length: 10–20 μm, purity: >90.0%) were purchased from Aladdin Chemistry Co. Ltd. and purified using a reflux method.

2.2. Materials Characterization

The structure of the prepared nanocomposite was characterised using X-ray diffraction (XRD, PANalytical AERIS-600) employing CuKα ($\lambda=1.5406\text{\AA}$) radiation. The surface morphology of the prepared nanocomposite was analysed using a field emission scanning electron microscope (SEM, JEM-2010, Japan). Electrochemical cyclic voltammetry (CV) and electrochemical impedance spectroscopy (EIS) were performed using Palm sense 4. Electrochemical measurements were taken with a double electrode configuration. In the double electrode configuration, a copper foil served as an electrode with 1 M of electrolyte H₂SO₄ and a ceramic separator at a voltage range of -0.4 V to 0.4 V. Then, the electrode was prepared with different compositions, as shown in Table 1.

Table 1. Variation of Material Composition

No.	Sample	Material Composition (MWCNT:rGO:TiO ₂)
1.	MWCNT-rGO	1:1:0
2.	TiO ₂	0:0:1
3.	MWCNT-rGO-TiO ₂ 60 %	1:1:3
4.	MWCNT-rGO-TiO ₂ 30 %	1:1:0.9

The composite was mixed with ethyl cellulose which served as a binding agent and ethanol with 60:25:15 portion to form a slurry. The copper foil was then coated with the slurry using a doctor blade method and dried at 80°C for 4-6 h until the layer had dried and become a thin layer of electrode. The CV and electrochemical-impedance-spectroscopy were done with two electrode cell setup using Palm Sense 4.

3. RESULTS AND DISCUSSION

3.1. XRD

Fig. 1 shows the XRD patterns. The pattern appeared with some diffraction peaks at 25.5° , 26.3° , 37.9° , 43.6° , 44.8° and 64.2° , corresponding to crystal planes of (002), (110), (200), (210), (211) and (301), respectively. Characteristic peaks at 25.5° and 43.6° indicated a crystalline MWCNTs (JCPDS Card No. 01-0646) [15]. The diffraction peak at 26.3° was identical to crystalline rGO (JCPDS Card No. 75-2078) [13]. Additionally, the peaks at 37.9° , 44.8° and 64.2° corresponded to crystalline pure TiO_2 nanorods with anatase phase (JCPDS Card No. 75-1749) [15, 17]. From the XRD patterns, it can be concluded that the MWCNTs (hexagonal) had 14.1 nm of crystalline. rGO and TiO_2 (hexagonal and tetragonal) had 10.3 and 25.3 nm of crystalline, respectively.

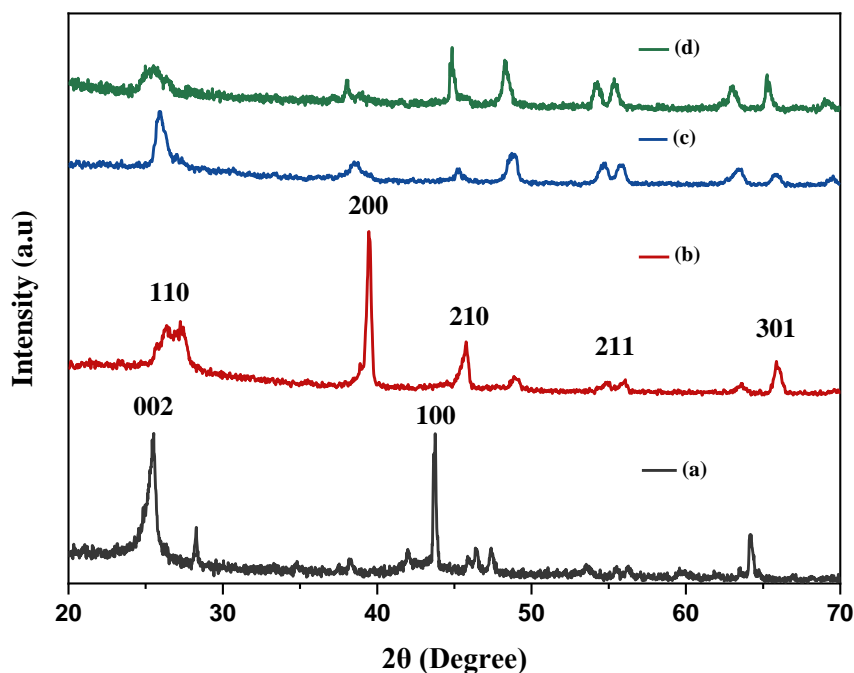


Figure 1. XRD pattern of the electrodes synthesized with: (a) MWCNT-rGO; (b) TiO_2 ; (c) MWCNT-RGO- TiO_2 60 %; (d) MWCNT-RGO- TiO_2 30 %.

Table 2. Structural parameters of MWCNT-rGO- TiO_2 electrode

Material	Phase	Lattice Parameters (\AA)	Crystalline Size (nm)	Strain	Dislocation Density ($\times 10^3 \text{ nm}^{-2}$)
MWCNTs	Hexagonal	$a = b = 1.553565,$ $c = 2.32642,$ $\alpha = \beta = \gamma \neq 90^\circ$	14.1	0.044728	5.0229
rGO	Hexagonal	$a = b = 1.5499,$ $c = 2.2522,$ $\alpha = \beta = \gamma \neq 90^\circ$	10.3	0.058878	9.4259

		a = b = 2.01906			
TiO ₂	Tetragonal	c = 3.7666	25.3	0.017922	1.5622
Nanorods		$\alpha = \beta = \gamma = 90^\circ$			

3.2. Surface Morphology

SEM imaging was used to characterise the surface morphology of the electrode. The surface morphology of the prepared MWCNT-rGO-TiO₂ electrode is shown in Fig.2. Fig. 2 (a) presents the SEM images of the MWCNT-rGO electrode on the aluminium foil. The MWCNTs and rGO materials were still agglomerated and there were no mesopores formed at the electrode. Fig. 2 (b) shows a crystalline TiO₂ covering the area, however, from observations, it did not have sufficient surface area as a supercapacitor. Fig. 2 (c) shows the composite MWCNT-rGO-TiO₂ 60%, which was beginning to show the particle structure of the material; no agglomeration occurred and mesopores had begun to appear, theoretically improving the surface area. Fig. 2 (d) shows significant morphological changes along with changes in the composition of the electrodes; the MWCNTs and rGO materials had formed mesopores. However, TiO₂ crystals also began to form and blend with the electrode. For the reason, metal oxide is important part for the functions during the faradaic process, the mesopores and the formation of TiO₂ is useful for increasing the capacitance of a supercapacitor.

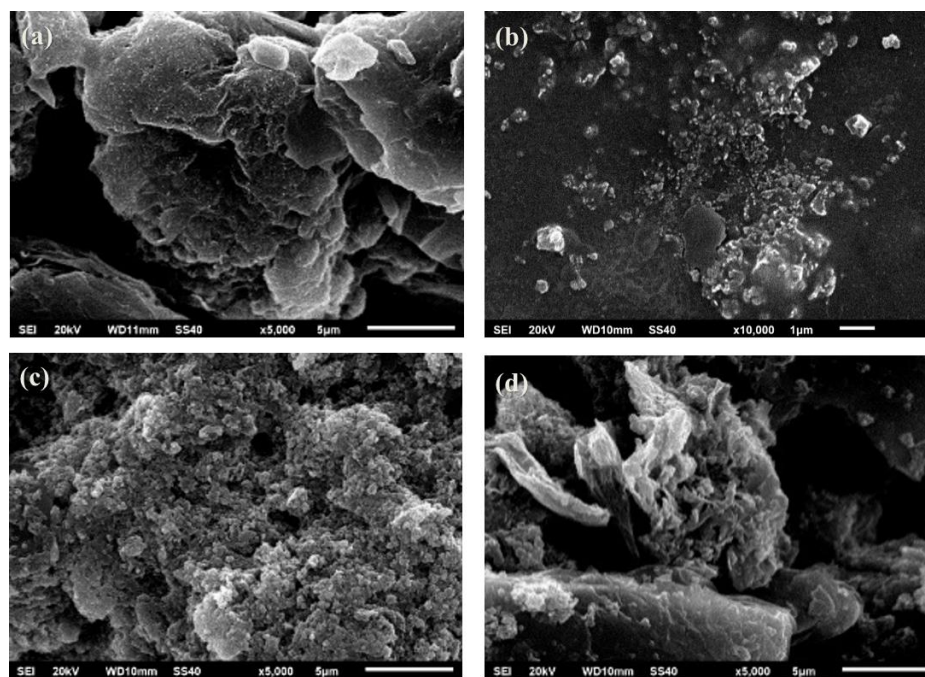


Figure 2. SEM images for: (a) MWCNT-rGO; (b) TiO₂; (c) MWCNT-RGO-TiO₂ 60%; (d) MWCNT-RGO-TiO₂ 30%.

3.3. Electrochemical Studies

CV was employed to analyse the electrochemical behaviour of the electrodes. The CV of MWCNT-rGO-TiO₂ at scan rates (10 mV/s) within a range of -0.4V to 0.4V is shown in Fig 3. The appearance of a non-rectangular shape in the CV shape indicates the pseudocapacitive behaviour of the titanium oxide nanoparticles. The current under the curve increased steadily with the scan rate, including at higher scan rates, the supercapacitors was deformed at high scan rates and also two small redox reaction peaks [17]. The observed non-linear current response to the scanning rate may have been due to the presence of cell terminal resistance, which can change the current reaction to the applied potential during the measurement process. The specific capacitance of the cell terminal material was determined by the specific capacitance equation. Fig. 3 shows that MWCNT-rGO-TiO₂ 30% had the highest specific capacitance at 168.64 Fg⁻¹; the specific capacitance of MWCNT-rGO-TiO₂ 60%, the MWCNT-rGO and MWCNT-rGO-TiO₂ 100% electrodes were 90.815 Fg⁻¹, 3.436 Fg⁻¹ and 1.963 Fg⁻¹, respectively. The energy and power densities calculated using different equation, the result of value supercapacitor was as follows MWCNT-rGO-TiO₂ 30%, MWCNT-rGO-TiO₂ 60%, MWCNT-rGO and MWCNT-rGO-TiO₂ 100%: (15 Whkg⁻¹, 337.5 Wkg⁻¹); (8 Whkg⁻¹, 180 Wkg⁻¹); (0.3 Whkg⁻¹, 6.75 Wkg⁻¹); (0.17 Whkg⁻¹, 3.83 Wkg⁻¹). The equations to calculate the value of specific capacitance, power density and energy density are shown in equations 1, 2 and 3, respectively.

$$C_s = \frac{dQ}{dV} = \frac{1}{mv\Delta V} \int_{V_1}^{V_2} I(V)dV \dots\dots (1)$$

$$E = \frac{1}{2} \left[\frac{C_s \cdot \Delta V^2}{3.6} \right] \dots\dots (2)$$

$$P = \frac{3600 E}{\Delta t} \dots\dots (3)$$

where C_s is specific capacitance (F/g), I is current density (mA g⁻¹), m is mass of the electrode, Δt is the discharge time (s), ΔV is the drop of voltage observed for a complete discharge, E is the energy density (Whkg⁻¹) and P is the power density (Wkg⁻¹).

The electrodes using carbon materials and metal oxide such as MWCNT-rGO-TiO₂ can be classified as hybrid supercapacitors, the low MWCNT-rGO and TiO₂ conductivity limited the current density of the electrode and caused significant polarisation on the supercapacitor during charge/discharge at specific current densities. Electrode polarization is the difference between the anodic and cathodic peak potentials (Fig. 3). EIS measurements were taken for the variation of all electrodes to obtain the resistance values between the supercapacitors. The Nyquist plot was obtained through EIS measurements using a Palm Sense 4 device and an equivalent circuit was obtained which was used to calculate the electrical resistance between the internal elements in this supercapacitor.

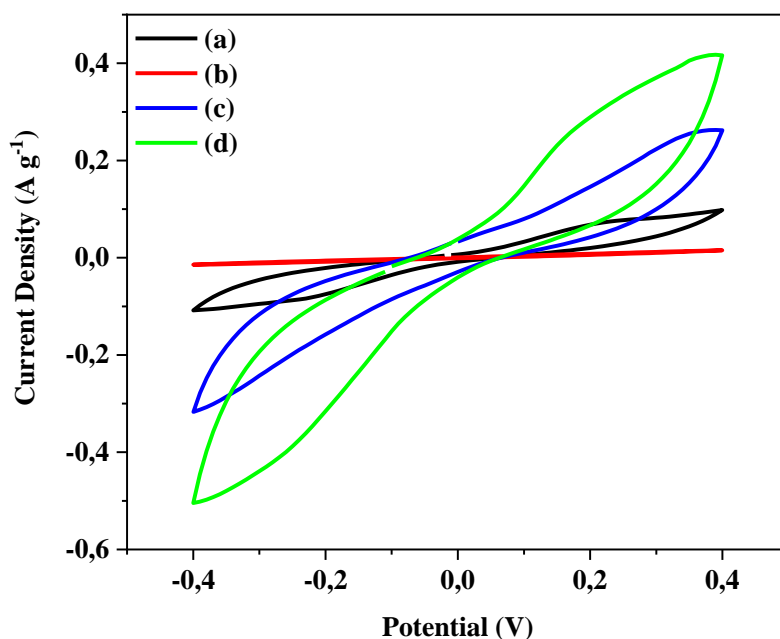


Figure 3. CV plot of electrodes for: (a) MWCNT-rGO; (b) TiO₂; (c) MWCNT-RGO-TiO₂ 60%; (d) MWCNT-RGO-TiO₂ 30%.

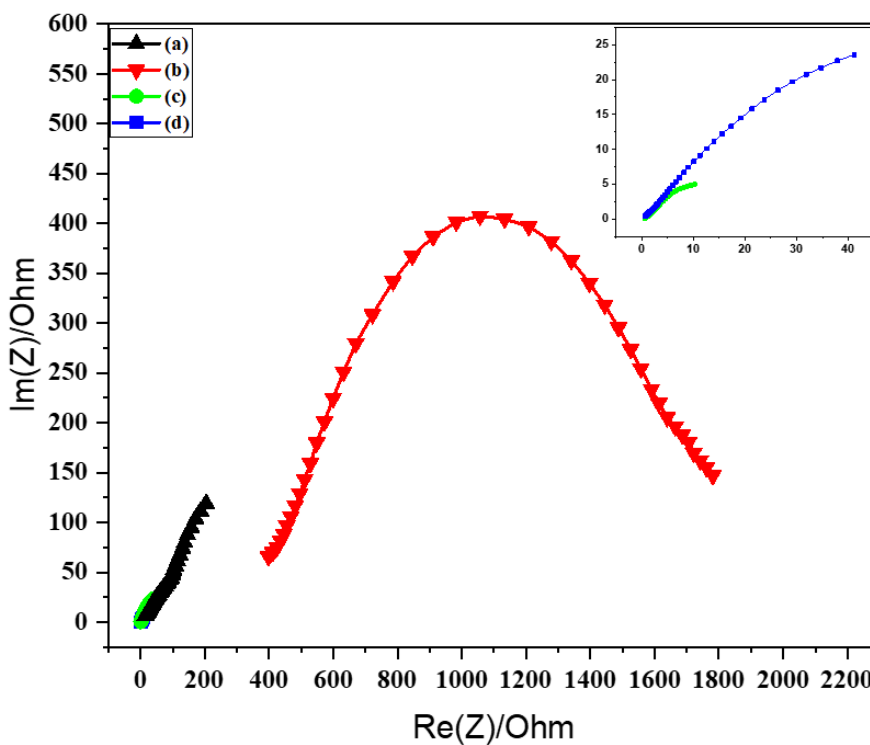


Figure 4. Nyquist plots for: (a) MWCNT-rGO; (b) TiO₂; (c) MWCNT-RGO-TiO₂ 60%; (d) MWCNT-RGO-TiO₂ 30% supercapacitors.

Based on the literature, fitting a Nyquist plot with an equivalent circuit (see inset in Figure 4) gives a serial resistance value of R_s (total cell resistance including electrode, electrolyte, and contact resistance) and a charge transfer resistance value of R_{ct} (at the electrode/electrolyte interface) [16]. Sequentially, the calculated values for (R_s , R_{ct}) were (7.49 Ω , 114.86 Ω), (373.12 Ω , 1455.1 Ω), (0.6 Ω , 5.21 Ω), (0.65 Ω , 0.75 Ω) for the MWCNT-rGO, TiO₂, MWCNT-rGO-TiO₂ 60%, and MWCNT-rGO-TiO₂ 30% supercapacitor devices, respectively. The MWCNT-rGO-TiO₂ 30% supercapacitor was the lowest among the other composition. This confirmed the usefulness of the composite electrode MWCNT-rGO-TiO₂ for reducing the internal resistance among elements and improving the ion diffusion and transport toward the single materials electrode [16].

Table 3 shows both our and other research methods and the type of electrolyte specific capacitance and energy density values obtained. We produced significant specific capacitance and energy density in our supercapacitors. Compared to other studies, the capacitance and energy density of our supercapacitors had convincing values. The specific capacitance of MWCNT-rGO-TiO₂ 30% (168 Fg^{-1}) was higher than that for TiO₂/rGO/TiO₂ (83 Fg^{-1}) and the carbon nanohorns and TiO₂ nanoflower (168 Fg^{-1}). The energy density value was 15 Whkg^{-1} for MWCNT-rGO-TiO₂ 30%, 15 Whkg^{-1} for CNT/TiO₂ and 20 Whkg^{-1} for TiO₂/rGO/Ni(OH)₂/NF. Future studies can examine electrodes more comprehensively to obtain better capacitance and energy density values [19-24].

Table 3. Electrochemical characteristic of the supercapacitors.

Material	Method	Electrolyte	Capacitance (Fg^{-1})	Energy Density (Whkg^{-1})	Ref
MWCNT-rGO-TiO ₂ 30%	Hydrothermal	1 M H ₂ SO ₄	168	15	This study
CNT/Ni@TiO ₂	Hydrothermal	H ₃ PO ₄	549	336	[18]
CNT/TiO ₂	CVD	PVA-H ₃ PO ₄ gel	26	11	[19]
PTP/PANI/TiO ₂	Oxidative chemical polymerisation	1 M H ₂ SO ₄	265	4	[20]
TiO ₂ /rGO/TiO ₂	Sol-gel	1 M KOH	83	-	[21]
TiO ₂ nanowire	Hydrothermal	1 M NaOH	57	1.3	[22]
Carbon nanohorns and TiO ₂ nanoflower	Solvothermal	6 M KOH	164	-	[23]
TiO ₂ /rGO/Ni(OH) ₂ /NF	Hydrothermal	1 M KOH	374	20	[24]

4. CONCLUSION

We fabricated MWCNTs, rGO and TiO₂ based hybrid supercapacitors. The hybrid and individual materials were obtained via SEM and XRD methods. A combination of MWCNTs, rGO and TiO₂ affected the morphology, structure and single material of the supercapacitors. The combination of materials caused the electrodes to form mesopores and nanomaterial structures. The combination of carbon material and metal oxides formed a new composite which increased the electrochemical value, making the supercapacitor more efficient due to the role of redox and pseudocapacitive reactions that occurred while charging and discharging hybrid supercapacitors. MWCNT-rGO-TiO₂ 30% had the highest electrochemical values with values of 168 F g⁻¹, 15 Whkg⁻¹, 337.5 Wkg⁻¹, 0.65 Ω and 0.75 Ω for specific capacitance, power density, energy density, R_s and R_{ct}, respectively. The results of the MWCNT-rGO-TiO₂ composite can be further studied to optimize its use as a supercapacitor.

ACKNOWLEDGEMENT

We would thank to Physics Department of Science and Mathematics Faculty, Diponegoro University and Bionano Technology Laboratory, Diponegoro University for funding our research.

References

1. E.B.O. Sihite, Stepanus and Budiarto, *IOP Conf. Ser.: Mater. Sci. Eng.*, 725 (2020) 012042.
2. M. Shahbaz, B.A. Topcu, S.S. Sarıgül and X.V. Vo, *Renewable Energy*, 178 (2021) 1370.
3. V. Choudhary and A. Gupta, *Polym. Compos.*, (2011) 65.
4. X. Liu, L. Xue, Y. Lu, Y. Xia and Q. Li, *J. Electroanal. Chem.*, 862 (2020) 3.
5. A.A. Iurchenkova, E.O. Fedorovskaya, I.P. Asanov, V.E. Arkhipov, K.M. Popov, K.I. Baskakova and A. V. Okotrub, *Electrochim. Acta*, 335 (2020) 135700.
6. E. Taer, A. Putri, R. Farma, Awitdrus, R. Taslim, Apriwandi, Agustino and D.A. Yusra, *Mater. Today: Proc.*, 44 (2020) 3241.
7. A. Karaphun, C. Phrompet, W. Tuichai, N. Chanlek, C. Sriwong and C. Ruttanapun, *Mater. Sci. Eng., B*, 264 (2021) 114941.
8. L. Jin, K. Wei, Y. Xia, B. Liu, K. Zhang, H. Gao, X. Chu, M. Ye, L. He and P. Lin, *Mater. Today Energy*, 14 (2019) 100348.
9. M.F. El-Kady, M. Ihns, M. Li, J.Y. Hwang, M.F. Mousavi, L. Chaney, A.T. Lech and R.B. Kaner, *Proc. Natl. Acad. Sci. U. S. A.*, 112 (2015) 4233.
10. H.J. Choi, J.H. Kim, H.K. Kim, S.H. Lee and Y.H. Lee, *Electrochim. Acta*, 208 (2016) 202.
11. M.S. Lal, R. Badam, N. Matsumi and S. Ramaprabhu, *J. Energy Storage*, 40 (2021) 102794.
12. J. Kim, J.H. Eum, J. Kang, O. Kwon, H. Kim and D.W. Kim, *Sci. Rep.*, 11 (2021), 1.
13. R. Rajagopal and K.S. Ryu, *Appl. Catal., B*, 236 (2018) 125.
14. S. Sundriyal, V. Shrivastav, M. Sharma, S. Mishra and A. Deep, *J. Alloys Compd.*, 790 (2019) 377–387.
15. N.T. Abdel-Ghani, G.A. El-Chaghaby and F.S. Helal, *J. Adv. Res.*, 6 (2015) 405.
16. X. Su, Q. He, Y. E. Yang, G. Cheng, D. Dang and L. Yu, *Diamond Relat. Mater.*, 114 (2021) 108168.
17. E. Nirmala Devi, M. Chandra Sekhar, and N.V.S.S. Seshagiri Rao, *AIP Conf.*, 2417 (2021) 020020.

18. R. Mendoza, M. Al-Sardar, A.I. Oliva, G. Robledo-Trujillo, V. Rodriguez-Gonzalez, A. Zakhidov and J. Oliva, *J. Phys. Chem. Solids*, 155 (2021) 110128.
19. T. Li, Y. Wu, Q. Wang, D. Zhang, A. Zhang and M. Miao, *J. Mater. Sci.*, 52 (2017) 7733.
20. A.K. Thakur, R.B. Choudhary, M. Majumder and M. Majhi, *Ionics*, 24 (2018) 257.
21. P. Agharezaei, H. Abdizadeh and M.R. Golobostanfard, *Ceram. Int.*, 44 (2018) 4132.
22. C. Devi, R. Swaroop, A. Arya, S. Tanwar, A.L. Sharma and S. Kumar, *Polym. Bull.*, 3 (2021) 03737.
23. N. Ramesh Reddy, M. Mamatha Kumari, M.V. Shankar, K. Raghava Reddy, S. Woo Joo and T.M. Aminabhavi, *J. Environ. Manage.*, 277 (2021) 111433.
24. C. Zhao, P. Ju, S. Wang, Y. Zhang, S. Min and X. Qian, *Electrochim. Acta*, 218 (2016) 216.

© 2022 The Authors. Published by ESG (www.electrochemsci.org). This article is an open access article distributed under the terms and conditions of the Creative Commons Attribution license (<http://creativecommons.org/licenses/by/4.0/>).